Complex dynamical behaviors in a memcapacitor–inductor circuit

M. Kountchou[1,2] · V. R. Folifack Signing[1,2,3] · R. L. Tagne Mogue[1,2,3] · J. Kengne[3] · Saïdou[2,4]

Abstract

In this present contribution, a simple chaotic oscillator based on a memcapacitor with only one equilibrium point is reported. The proposed oscillator consists of an inductor (only storage element) and a nonlinear active memcapacitor which is the key component responsible for the complex behaviors exhibited by the circuit. The resulting mathematical model is a simple jerk-type equation system that is easy to manipulate both analytically and numerically. The numerical results reveal the emergence of a plethora of phenomena such as period-doubling bifurcations, antimonotonicity, offset-boosting, and multistability giving rise to several kinds of coexisting attractors among which the coexistence of six stable states. The PSpice investigations confirm the real feasibility of the proposed circuit. The complexity of the phenomena and behaviors observed make the particularity of the proposed memcapacitor–inductor circuit and thus constitutes an enriching contribution in nonlinear dynamics.

Keywords Simple chaotic circuit · Memcapacitor · Antimonotonicity · Offset-boosting · Multistability · Pspice simulations

1 Introduction

The existence of the memristor as the fourth electronic component having a memory next to the resistor, capacitance, and inductor was deduced in 1971 by Chua [1]. Many applications in nonlinear circuits have been realized through the memristor in the growing interest of nonlinear science [2–6]. Later in 2009, Di Vental et al. formally defined the three pinch hysteresis loops of each element combining two consecutive state variables when an alternative source is applied to them, notably the current–voltage for the memristor, charge–voltage for the memcapacitor and current-flux for the meminductor [7]. Several works on chaotic oscillations based on the memristor have been investigated. Memristor models are used to replace the nonlinear negative resistance of the Chua circuit with that of the quadratic, cubic, piecewise linear model [8–10]. Using some models derived from HP memristor a chaotic circuit was explored in [11, 12]. In 2016, an application in cryptography was analyzed using a chaotic system based on the memristor [13]. In the same year, an optimal synchronization on a memristor circuit was investigated [14]. Unlike the memristor, few works have been investigated with the memcapacitor and the meminductor. Notably, some dynamic systems based on memcapacitor and meminductor are designed and studied through mathematical models [15–18], and equivalent circuits [19–25]. The smooth cubic nonlinearities used for memcapacitor and meminductor are proposed respectively by Fitch et al. [15], and Yuan et al. [26]. Very recently in 2019, a chaotic oscillator based on memcapacitor and meminductor has been proposed and investigated [27]. In that same year, Yuan et al. also proposed a new model of memcapacitor and its corresponding circuit used in a chaotic oscillator explored analytically and experimentally [28]. The previous works present simple chaotic circuits having at least three components. Another simple chaotic system based on

✉ M. Kountchou
    kountchounoube@yahoo.fr

1   Unité de Recherche de Matière Condensée, d'Electronique et de Traitement du Signal (URMACETS), Department of Physics, University of Dschang, P.O. Box 67, Dschang, Cameroon

2   Nuclear Technology Section, Institute of Geological and Mining Research, P.O. Box 4110, Yaoundé, Cameroon

3   Unité de Recherche de Laboratoire d'Automatique et Informatique Appliquée (URAIA), Department of Electrical Engineering, IUT-FV Bandjoun, University of Dschang, Dschang, Cameroon

4   Nuclear Physics Laboratory, Faculty of Science, University of Yaounde I, P.O. Box 812, Yaoundé, Cameroon

meminductor was also proposed in 2017 by Birong et al. [29], whose authors investigated the complete dynamics.

Very recently, Ngoumkam and Kengne have proposed a minimal three-term chaotic Jerk system consisting of two linear terms and single hyperbolic sine nonlinearity. The authors have shown that the system can exhibit a coexistence of six different solutions for a set of parameters of the system [30]. Tchinga et al., in their work proposed the simplest chaotic circuit of Hartley's oscillator family consisting of two components including an inductor and a JFET [31]. They also reported a simple autonomous chaotic oscillator with five jerky type components, considered to be the simplest of its kind, using a single operational amplifier [32]. In these works [27, 28], the authors have not carried out detailed dynamic studies. Very recently, Joshi and his collaborators presented a simple oscillator which can be both chaotic and hyperchaotic with a sine hyperbolic nonlinearity [33]. The authors also presented a simple Jerk system with hyperbolic sine nonlinearity which can be either from the category of hidden attractors or self-excited attractors according on the nature of the equilibrium points [34]. As a result, Joshi and Ranjan proposed a new simple chaotic oscillator consisting of a single operational amplifier with tank circuit to generate a chaotic waveform [35].

Since the challenge nowadays is to propose oscillators that are very simple both in their circuits and their equations, and presenting complex dynamic behaviors, in this paper a simple circuit consisting of an inductor and a memcapacitor that can exhibit a plethora of dynamic phenomena is proposed. This work is original and highlights the following innovations:

(a) The proposed circuit is simple, consisting only of an inductor and a nonlinear active memcapacitor;The proposed circuit is simple, consisting only of an inductor and a nonlinear active memcapacitor;

(b) The proposed circuit although simple, presents chaos and very complex dynamic behaviors including antimonotonicity, offset-boosting, multistability, and many others;

(c) The mathematical model resulting from the proposed circuit is a simple jerk-type equation system that is easy to manipulate both analytically and numerically;

(d) Multistability gives rise to the coexistence of two, three, four, and even six attractors, which is usually difficult to find in 3D jerk systems.

Considering the standard for the publication of new chaotic systems mentioned by Sprott in 2011 [36], the new proposed system satisfies all the three publication criteria and for this purpose enriches the literature on dynamic circuits and systems based on controlled-charge memcapacitor. The rest of this article is organized as follows: in Sect. 2, the mathematical model of a charge-controlled memcapacitor is proposed and used for designing a simple chaotic oscillator. Based on the mathematical model of the proposed circuit, its dynamics analysis is performed. Basic properties of the system are explored analytically in Sect. 3. In Sect. 4, bifurcation diagrams, Lyapunov stability diagrams for an overall system view, antimonotonicity, and multistability are investigated and explored. PSpice studies are explored in Sect. 5 for the validation of the proposed circuit and finally, a conclusion of the work in Sect. 6.

2 Memcapacitor model and a simple memcapacitor-based chaotic circuit

2.1 Memcapacitor model

In accordance with the general definition reported in Ref. [7], the charge-controlled memcapacitor is described as:

$$\begin{cases} v_m(t) = C^{-1}(\sigma_m(t))q_m(t), \\ \dot{\sigma}_m(t) = q_m(t), \end{cases} \tag{1}$$

where $v_m(t)$ is the voltage across the memcapacitor, $q_m(t)$ the charge passing through the memcapacitor at time t, $\sigma_m(t)$ the integral of $q_m(t)$, and C^{-1} the inverse memcapacitance. In this paper, we define C^{-1} according to the charge $q_m(t)$ and the non-linear element $\sigma_m(t)$ as follow:

$$C^{-1} = \frac{A_1}{q_m}\sigma_m(t) + A_2\sigma_m^4(t) - A_3, \tag{2}$$

By substituting Eq. (2) in Eq. (1), we obtain the expression of the proposed memcapacitor model which is described as follows (time dependence was intentionally omitted for simplicity):

$$\begin{cases} v_m = \left(\frac{A_1}{q_m}\sigma_m + A_2\sigma_m^4 - A_3\right)q_m, \\ \dot{\sigma}_m = q_m, \end{cases} \tag{3}$$

where A_1, A_2, and A_3 are positive real constants. In order to test the property of this proposed memcapacitor, we set $A_1 = 1$, $A_2 = 0.1$, $A_3 = 1$ and $q_m(t) = U\sin(2\pi ft)$, by varying the frequency (f), amplitude (U) and initial conditions ($\sigma_m(0)$). The simulation results of the $v_m - q_m$ hysteresis curve are illustrated in Fig. 1. From this Fig. 1, a pinched hysteresis loop and a hysteresis collapse with increasing frequency (f), amplitude (U) and initial conditions ($\sigma_m(0)$) of the alternating voltage source are clearly observed and the considered memcapacitor faithfully respects the conditions described in [7], these curves conform to the definition of the negative memcapacitor's characteristics [37].
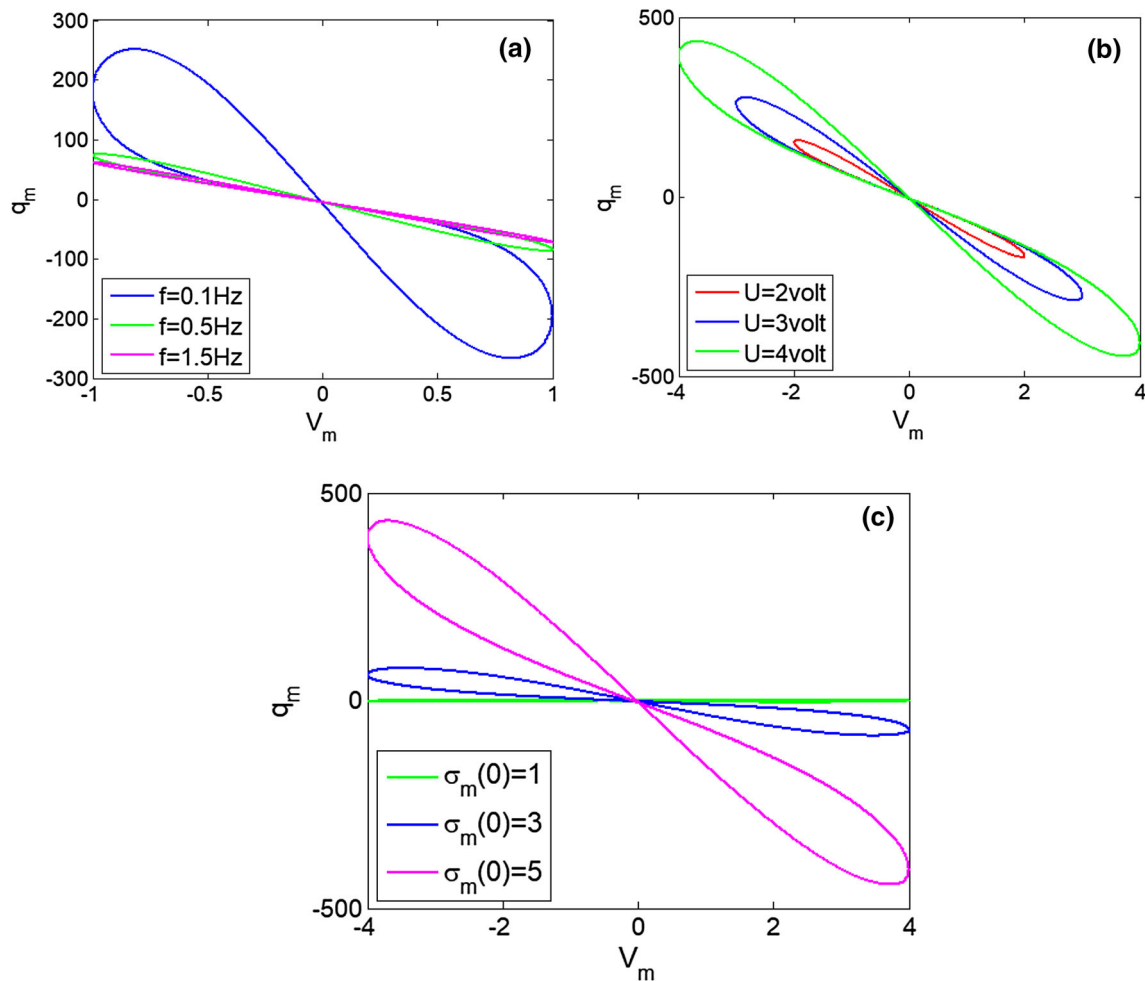
Fig. 1 $q_m - v_m$ hysteresis loop of the novel memcapacitor in different situation: **a** for f = 0.1 Hz, f = 0.5 Hz, and f = 1.5 Hz, **b** for U = 2 v, U = 3 v, and U = 5 v; **c** for $\sigma_m(0) = 1$, $\sigma_m(0) = 3$, and $\sigma_m(0) = 5$. Obtained for the fixed parameters $A_1 = 1$, $A_2 = 0.1$, and $A_3 = 1$

2.2 A simple memcapacitor-based chaotic circuit

Based on the proposed memcapacitor model in Eq. (3), a simple chaotic oscillator consisting of an inductor and a memcapacitor is designed as shown in Fig. 2. Since the memcapacitor is the central element of the proposed circuit as responsible for the autonomy and also the complex behavior of the system thanks to its nonlinearity; it constitutes the only active element [38]. By applying
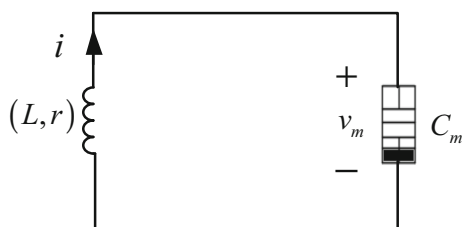
Fig. 2 The proposed memcapacitor-based chaotic oscillator where r is the internal resistance of the inductor

Kirchhoff's laws to the circuit of Fig. 2 and taking the charge q_m on the memcapacitor, the current i through the inductor and the internal state variable σ_m of the memcapacitor as state variables, the following differential equations of the circuit are obtained:

$$
\begin{aligned}
\frac{d\sigma_m}{dt} &= q_m, \\
\frac{dq_m}{dt} &= i, \\
\frac{di}{dt} &= -\frac{r}{L}i - \frac{1}{L}v_m,
\end{aligned}
\tag{4}
$$

where $v_m = A_1\sigma_m + A_2\sigma_m^4 q_m - A_3 q_m$.

Considering $x_1 = \sigma_m$, $x_2 = q_m$, $x_3 = i$, $\alpha = \frac{A_3}{L}$, $\gamma = \frac{r}{L}$, $\beta = \frac{A_1}{L}$ and $\rho = \frac{A_2}{L}$, we obtain

$$
\begin{cases}
\dot{x}_1 = x_2, \\
\dot{x}_2 = x_3, \\
\dot{x}_3 = \alpha x_2 - \gamma x_3 - \beta x_1 - \rho x_2 x_1^4,
\end{cases}
\tag{5}
$$

where α, β, γ, and ρ represent the system setting parameters

(all are positive) and the dot represents differentiation with respect to time. By using simple mathematical rules, Eq. (5) can be written into the following simple jerk form

$$\dddot{x} = \alpha\dot{x} - \gamma\ddot{x} - \beta x - \rho\dot{x}x^4 \qquad (6)$$

3 Basic dynamical characteristic

3.1 Dissipativity and symmetry

The necessary condition to study the dissipation of our model (5) is expressed by the following equation [39–41]:

$$\nabla V = \frac{\partial\dot{x}_1}{\partial x_1} + \frac{\partial\dot{x}_2}{\partial x_2} + \frac{\partial\dot{x}_3}{\partial x_3} = -\gamma \qquad (7)$$

Since γ is a positive constant, the volume contraction rate Eq. (7) is always negative and the system (5) is dissipative. From Eq. (7), all trajectories are confined to space whose volume is zero [42] and, therefore, existing attractors can be chaotic.

Another important property is the symmetry, because it provides additional information about the dynamic behavior of the system. By performing the transformation $(x_1, x_2, x_3) \leftrightarrow (x_1, -x_2, -x_3)$ on the system (5), the solution remains the same. It implies that the system (5) is symmetric about the coordinate x_2 and x_3.

3.2 Stability of equilibrium point

To study the stability of equilibrium [43] point amounts to determine this point which is obtained by solving the system equation $\dot{x}_1 = \dot{x}_2 = \dot{x}_3 = 0$ in order to know if it is stable or unstable. The only equilibrium point is the origin $E_0 = (0, 0, 0)$. The Jacobian matrix of the system (5) around the fixed point E_0 is defined by:

$$J = \begin{bmatrix} 0 & 1 & 0 \\ 0 & 0 & 1 \\ -\beta & \alpha & -\gamma \end{bmatrix} \qquad (8)$$

whose characteristic equation is:

$$\lambda^3 + \gamma\lambda^2 - \alpha\lambda + \beta = 0 \qquad (9)$$

According to the Routh–Hurwitz criterion, the characteristic Eq. (9) is an opposite sign, therefore, the equilibrium point E_0 is always unstable whatever the set of system parameters'. For the range of system parameters $\alpha = 1$, $\beta = 0.5$, and $\rho = 1$, the eigenvalues, as well as the stability of fixed point are summarized in Table 1. In light of the results of Table 1, the eigenvalues, solutions of characteristic Eq. (9) are obtained in the form:

Table 1 Eigenvalues and stability of equilibrium point with fixed parameter $\alpha = 1$, $\beta = 0.5$, and $\rho = 1$

Control parameter γ	Eigenvalue	Stability
$\gamma = 0.1$	$\lambda_1 = -1.2362$	Unstable
	$\lambda_{2,3} = 0.56808 \pm 0.28594i$	
$\gamma = 0.3$	$\lambda_1 = -1.3323$	Unstable
	$\lambda_{2,3} = 0.51614 \pm 0.32999i$	
$\gamma = 0.5$	$\lambda_1 = -1.4376$	Unstable
	$\lambda_{2,3} = 0.46878 \pm 35785i$	
$\gamma = 0.8$	$\lambda_1 = -1.6125$	Unstable
	$\lambda_{2,3} = 0.40623 \pm 0.38086i$	
$\gamma = 1$	$\lambda_1 = -1.7399$	Unstable
	$\lambda_{2,3} = 0.36995 \pm 0.38795i$	

$$\begin{aligned} \lambda_1 &= -\eta \\ \lambda_{2,3} &= \vartheta \pm i\varphi \end{aligned} \qquad (10)$$

with positive constants η and ϑ. We note that λ_1 is real negative whereas the complex conjugate eigenvalues λ_2 and λ_3 are all real positive roots. Therefore, the fixed point E_0 is unstable saddle-focus equilibrium and the existing attractors can be classified as self-excited attractors [44, 45].
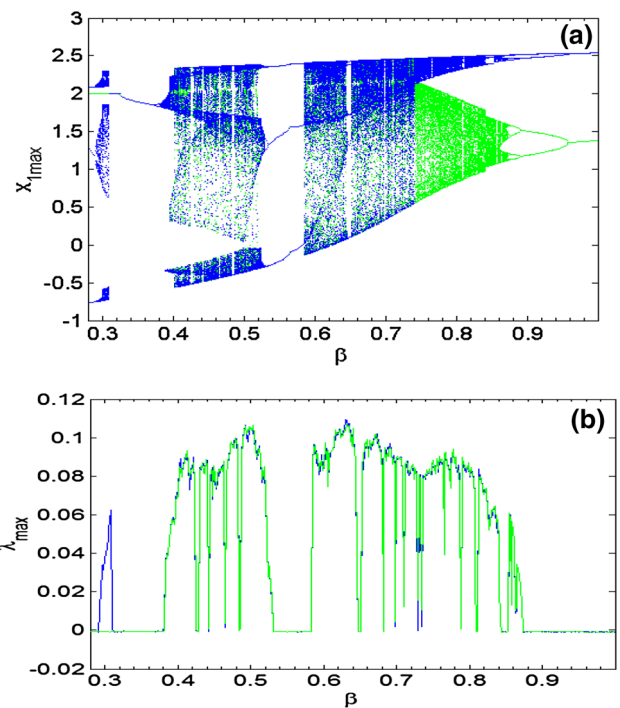
Fig. 3 Bifurcation diagrams **a** showing local maxima of the coordinate x_1 versus β and the corresponding largest **b** of Lyapunov exponents plotted in the range $0.28 \leq \beta \leq 1$ for $\alpha = 1$, $\gamma = 0.5$ and $\rho = 1$

4 Numerical simulations and dynamical behaviors

4.1 Bifurcation analysis and route to chaos

The system (5) is solved numerically using the standard four order Runge–Kutta algorithm and the largest Lyapunov exponent the Wolf algorithm [46] at $\Delta t = 10^{-3}$ s. The system reveals a complex and varied dynamic that reflects the bifurcation diagrams in Fig. 3(a) and their corresponding largest Lyapunov exponents of Fig. 3(b). It can be seen from Fig. 3 that chaos is obtained by period-doubling followed by a symmetry restoration when the parameter β is considered as a bifurcation control

Fig. 4 Phase portraits showing routes to chaos in the system for varying the control parameter β: **a** period-1 limit cycle for $\beta = 1$, **b** period-2 limit cycle for $\beta = 0.9$, **c** period-4 limit cycle for $\beta = 0.885$, **d** asymmetric chaos for $\beta = 0.8$, **e** symmetric chaos for $\beta = 0.7$, **f** period-3 limit cycle for $\beta = 0.56$, **g** symmetric chaos for $\beta = 0.4$, and **h** period-1 limit cycle for $\beta = 0.3$. Initial conditions $(x_1(0), x_2(0), x_3(0))$ are $(0, \pm 1, 0)$ for **a–d** and $(0, 1, 0)$ for **e–h**
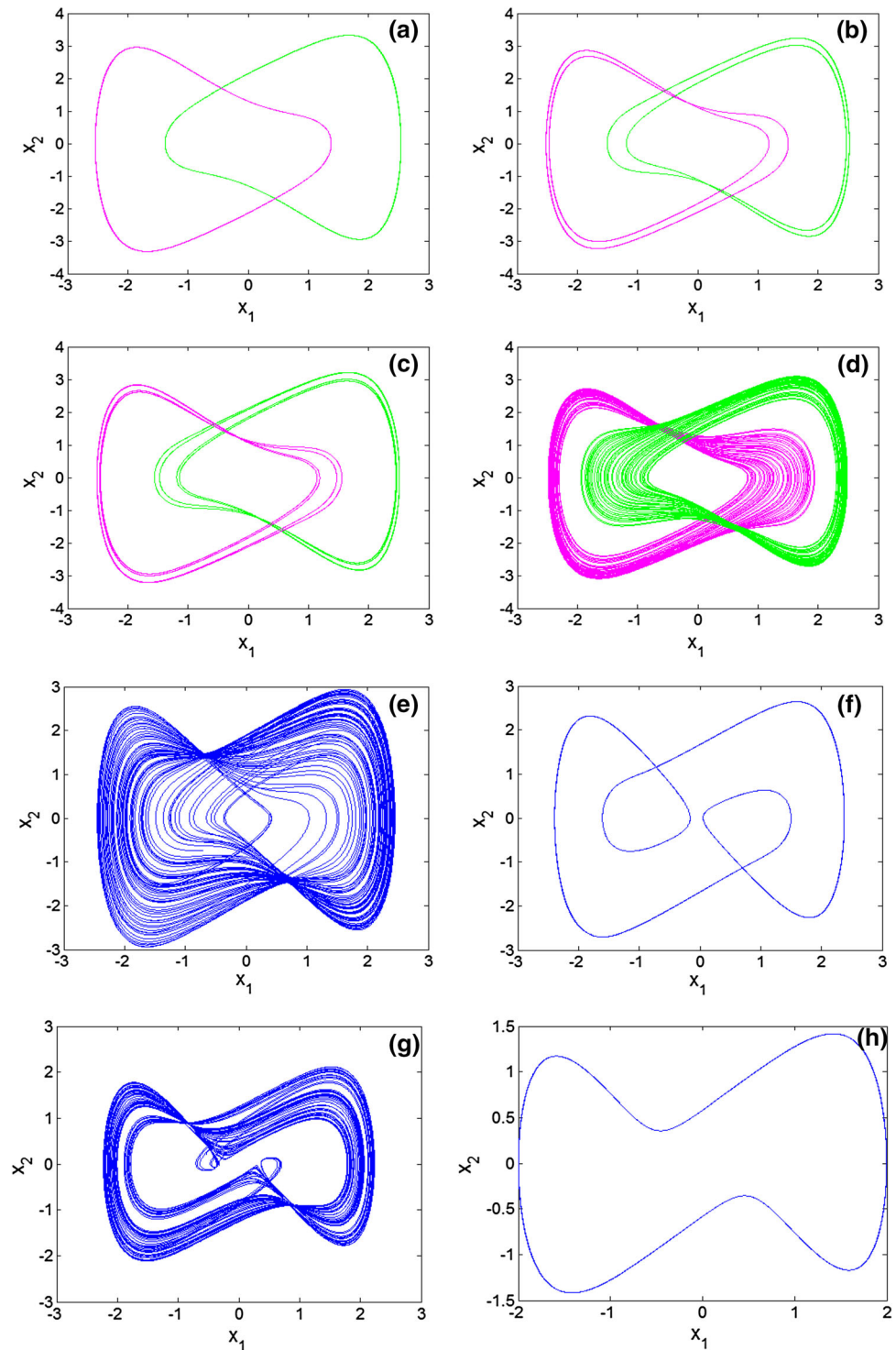
parameter. Two sets of data are superimposed and the color difference (blue by increasing the values of β and green by decreasing the values of the same parameter β) is observed to illustrate the symmetry property of the system. A good correspondence of periodicity of the system is observed on the bifurcation diagram and the largest Lyapunov exponent of Fig. 3. The transition to chaos is illustrated by the phase portraits in Fig. 4 when we consider the bifurcation diagram or the graph of Lyapunov exponent in green. In light of Fig. 4, the color difference (magenta and green) simply shows the asymmetrical behaviors. The attractors in blue are obtained when the symmetry of the system is restored.

The other parameters of the system in particular γ and α are also considered as bifurcation control parameters in a great interest to observe their influences on the dynamic behavior of the system. Thus, the bifurcation diagrams of Figs. 5(a) and 6(a) are obtained by plotting the local maxima of the state variable x_1 as a function of γ and α respectively. The corresponding graphs of Lyapunov exponents are shown in Figs. 5(b) and 6 (b) showing a good agreement between the periodicity of bifurcation diagrams. Moreover, striking phenomena are observed when a parameter a is introduced on the second line of the system (5). Note that this parameter a represents an intrinsic property that is highlighted during the design of the emulator circuit of the memcapacitor (see Sect. 5). Interesting behaviors are observed when it considered as a bifurcation control. Thus Fig. 7(a) shows two superimposed

bifurcations diagrams obtained by varying the bifurcation control parameter a in the range $1 \leq a \leq 12$ (see caption of Fig. 7). The corresponding graphs of Lyapunov exponents in Fig. 7(b) justify the correspondence between periodicity and the transition to chaos.
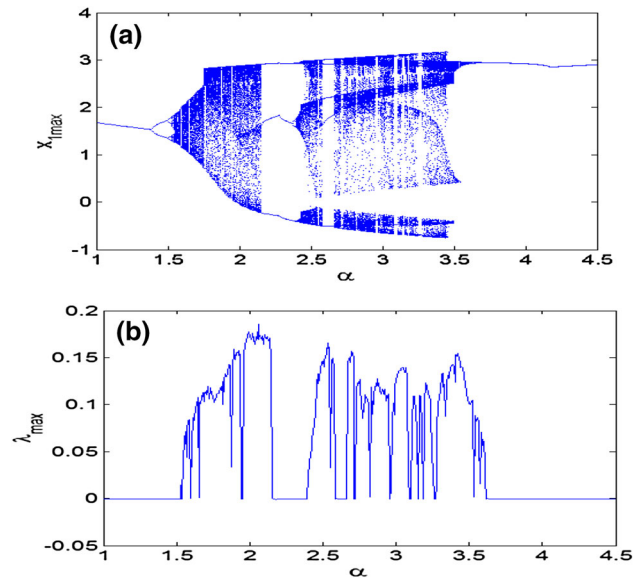

Fig. 6 Bifurcation diagrams a showing local maxima of the coordinate x_1 versus α and the corresponding largest b of Lyapunov exponents plotted in the range $1 \leq \alpha \leq 4.5$ for $\gamma = 0.8$, $\beta = 2$ and $\rho = 1$
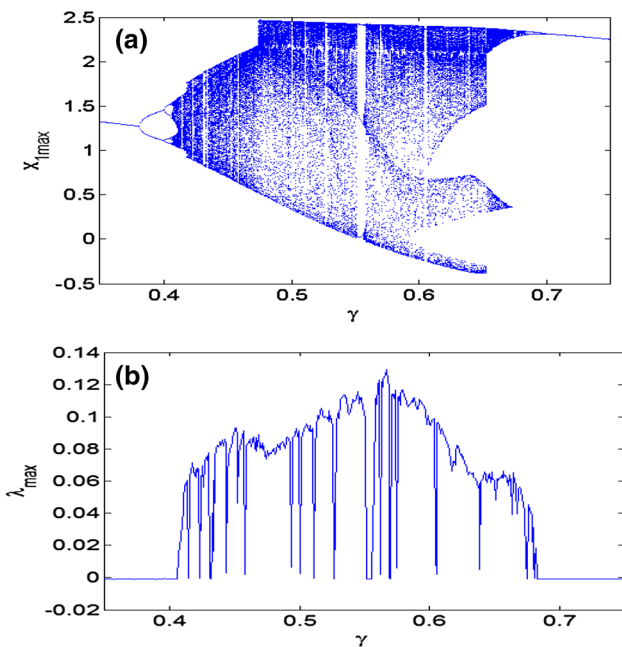

Fig. 5 Bifurcation diagrams a showing local maxima of the coordinate x_1 versus γ and the corresponding largest b of Lyapunov exponents plotted in the range $0.35 \leq \gamma \leq 0.75$ for $\alpha = 1$, $\beta = 0.7$ and $\rho = 1$
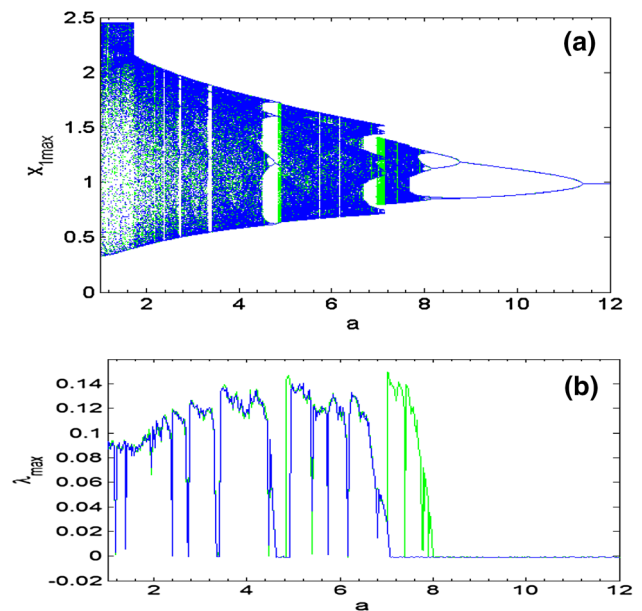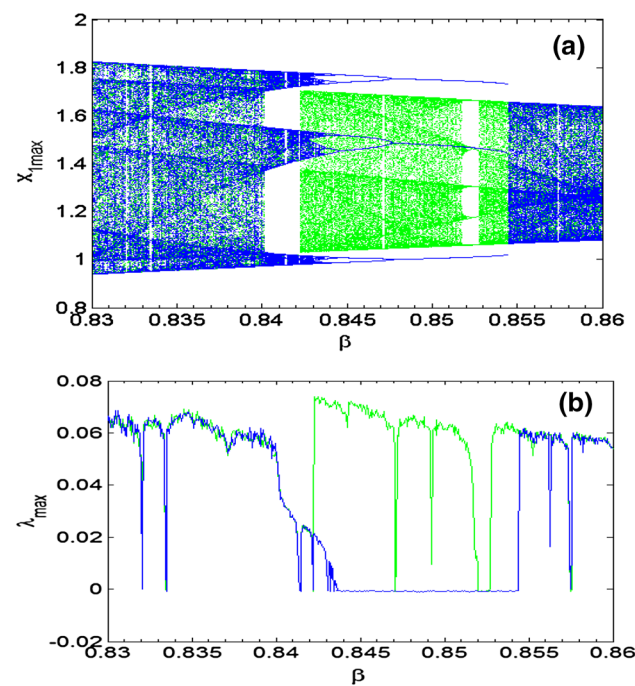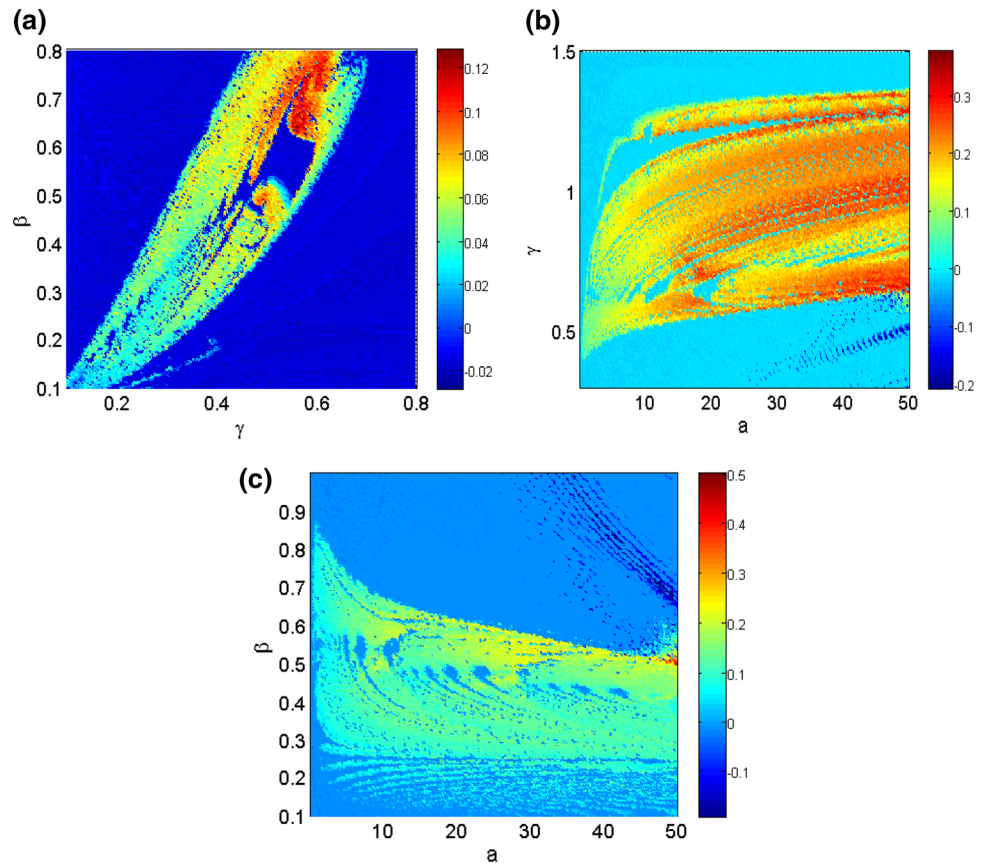

Fig. 7 Bifurcation diagrams a showing local maxima of the coordinate x_1 versus a and their corresponding largest b of Lyapunov exponents plotted in the range $1 \leq a \leq 12$ for $\alpha = 1$, $\gamma = 0.5$, $\beta = 0.7$ and $\rho = 1$

Fig. 8 Standard Lyapunov stability diagrams **a**, **b**, and **c** in the (γ, β), (a, γ), and (a, γ) plane obtained by scanning upward the values of control parameters where Lyapunov exponents are unable to discriminate individual behaviors. (Color figure online)


Fig. 9 Highlighting the hysteresis window of the bifurcation diagrams of Fig. 3 (**a**) and their corresponding largest **b** of Lyapunov exponents plotted in the range $0.83 \leq \beta \leq 0.86$ showing the different types of coexistences

Note that the color difference in Fig. 7 highlights both the symmetry and hysteresis behaviors of the system that will be exploited in the following sections. With regard to Figs. 5, 6 and 7, the same transition towards the chaos of Fig. 3 is observed when considering γ, α, and a as bifurcation control parameters.
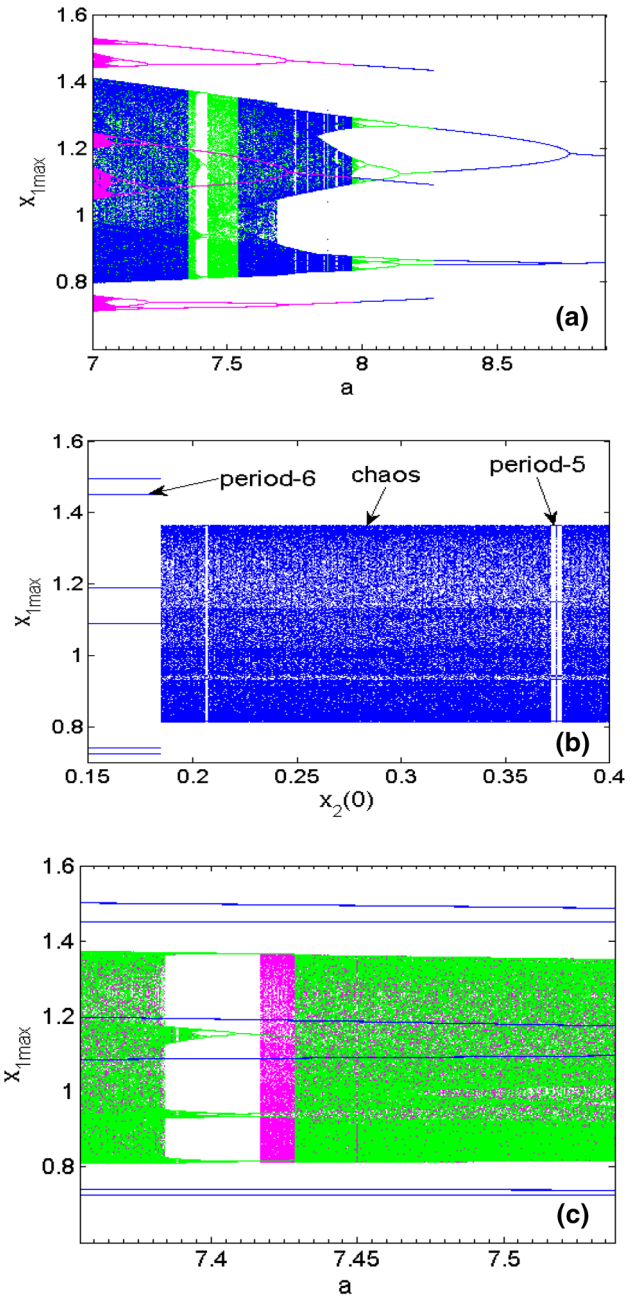
4.2 Lyapunov stability diagrams of the proposed system

It is always interesting to have a global idea of the dynamic behavior of a chaotic system for a better analysis of the system by studying the influence of one parameter on another. In the same line, we decided to study the influence of the different bifurcation control parameters presented previously. To better understand the type of dynamic behavior of the system (5), the Lyapunov exponent bands are enabled each time to characterize the different observed behaviors. Thus, Fig. 8(a) shows the effect of the parameter β on the parameter γ for the choice of the other parameters $\alpha = 1$ and $\rho = 1$ where the type of the dynamic behavior is a function at the same time both of the color and the value of the correspondence of the Lyapunov exponent. In light of the Lyapunov stability diagram of Fig. 8(a), the blue shadings correspond to the periodic
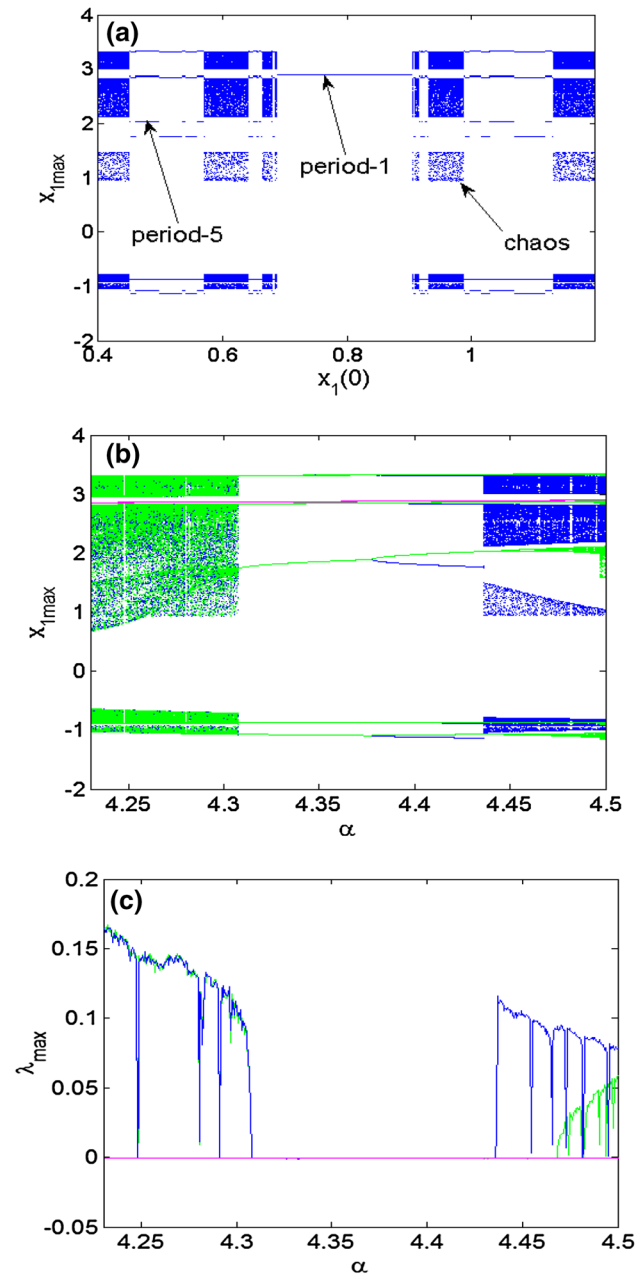
Fig. 10 a Bifurcation like sequence showing local maxima of the coordinate x_1 versus initial state $x_1(0)$ plotted in the range $0.4 \leq x_1(0) \leq 1.2$ while keeping $\alpha = 4.49$, $x_2(0) = 2$, and $x_3(0) = 5$; enlargement of bifurcation diagrams **b** of Fig. 5 and their corresponding largest **c** of Lyapunov exponents plotted in the range $4.23 \leq \alpha \leq 4.5$ showing the region in which the system experiences the coexistence of three symmetrical attractors

Fig. 11 a Enlargement of bifurcation diagrams a of Fig. 7 in the range $7 \leq a \leq 8.9$ showing the region in which the system develops the coexistence of six asymmetrical attractors; Bifurcation like sequence **b** showing local maxima of the coordinate x_1 versus initial state $x_2(0)$ plotted in the range $0.15 \leq x_2(0) \leq 0.4$ while keeping $a = 7.42$, $x_1(0) = 0.0$, and $x_3(0) = 0.0$; Enlargement of the bifurcation diagrams **c** of Fig. 10(b) in the interval $7.355 \leq a \leq 7.538$ showing the zone of coexistence of six asymmetrical solutions

attractors (negative Lyapunov exponents), the cyan marks attractors of high periodicity and more and more attractors of strong chaoticity for the data in dark red. When keeping set the parameters $\alpha = 1$, $\beta = 0.7$, and $\rho = 1$; the influence of the parameter a on γ is also observed in Fig. 8(b) which is strongly dominated by the high periodicity behaviors. The limit cycles of period-1 are weakly observed for this

set of parameters in blue, the periodicity increases in cyan until the chaotic behavior represented by the other colors. Similarly, the influence of the parameters a and β in Fig. 8(c) which presents a situation opposite to that of Fig. 8(b) because the periodic behavior dominates the

Fig. 12 Phase portraits illustrating the coexistence of two symmetric attractors (chaotic (**a**) and cycle limit of period-1 (**b**)) obtained for the set parameters $\beta = 0.3$, $\alpha = 1, \gamma = 0.5$, and $\rho = 1$. Initial conditions are $(0, 0.4, 0)$ and $(0, 1, 0)$ respectively
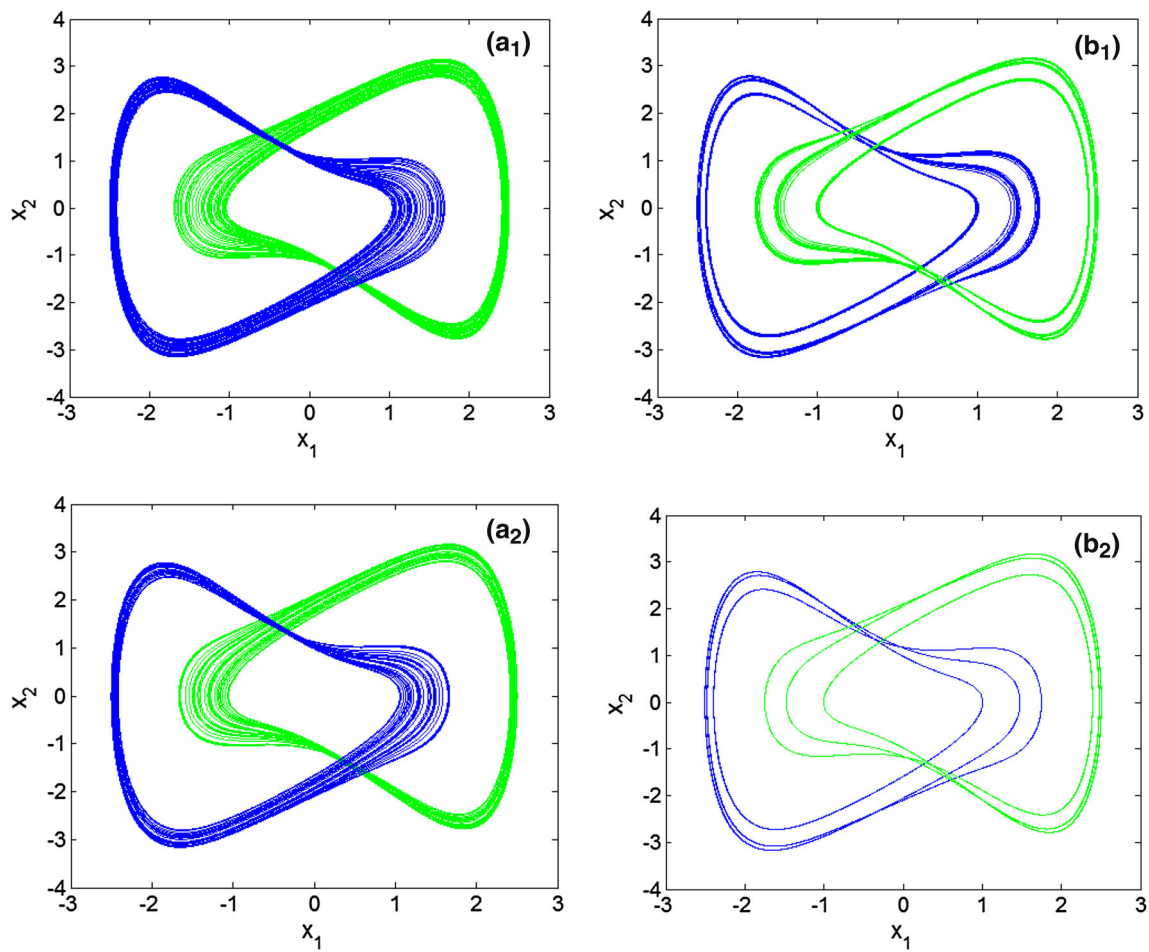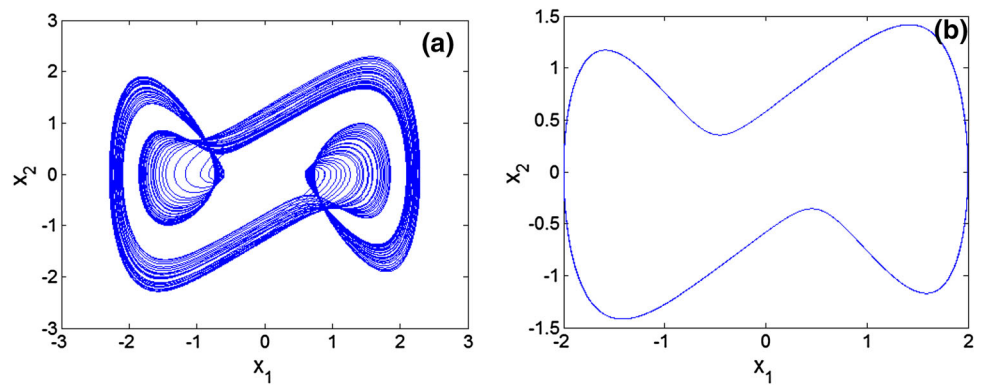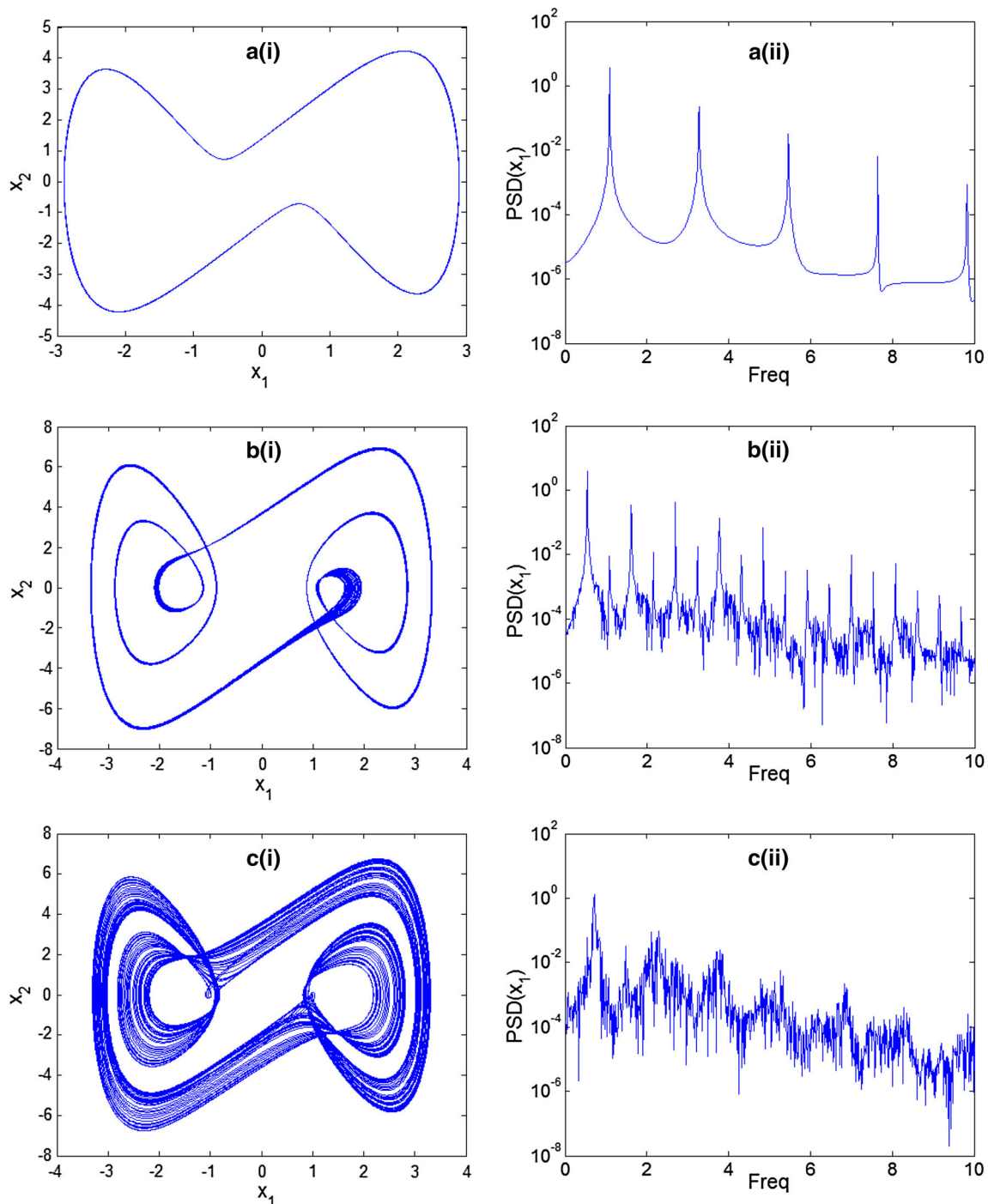

Fig. 13 Phase portraits illustrating the coexistence of four different types of attractors obtained for the fixed set $\alpha = 1, \gamma = 0.5$, $\rho = 1, x_1(0) = 0.0$, and $x_3(0) = 0.0$: four different chaotic attractors for $\beta = 0.8425$, $x_2(0) = \pm 0.4$ (**a₁**) and $x_2(0) = \pm 0.7$ (**b₁**); two chaos with two limit cycles of period-3 for $\beta = 0.85$, $x_2(0) = \pm 0.4$ (**a₂**) and $x_2(0) = \pm 0.7$ (**b₂**); two limit cycles of period-5 with two limit cycles of period-3 $\beta = 0.8526$, $x_2(0) = \pm 0.4$ (**a₃**) and $x_2(0) = \pm 0.7$ (**b₃**)

chaotic one by the strong cyan coloration. The rest of parameters are $\alpha = 1$, $\gamma = 0.5$, and $\rho = 1$.

Let us note that this way of representation is very important for the good control of the dynamic behavior of

the system (5) and even for practical studies on the choice of the parameters of the system while having an idea on the dynamic behavior. In the literature, these Lyapunov stability diagrams are used namely in [47, 48].

Fig. 14 Phase portraits in the (x_1, x_2) plan and their corresponding spectral power density obtained for the parameters of the system $\beta = 2, \gamma = 0.8$, $\rho = 1$, and $\alpha = 4.49$ illustrating the coexistence of three symmetrical solutions: **a** limit cycle of period-1 with two different chaotic attractors (**b**, **c**). Initial conditions are (0.8, 2, 5),(0.5, 2, 5), and (0.6, 2, 5) respectively

4.3 Multistability and offset boosting

Unlike the bifurcation diagram and the largest of Lyapunov exponent where a so-called bifurcation parameter is varied for a qualitative analysis, there is an unusual and striking phenomenon which is obtained by varying only the initial conditions for the same set of given parameter's system and commonly called multistability or coexistence of several stable states (attractors). Each attractor that coexists
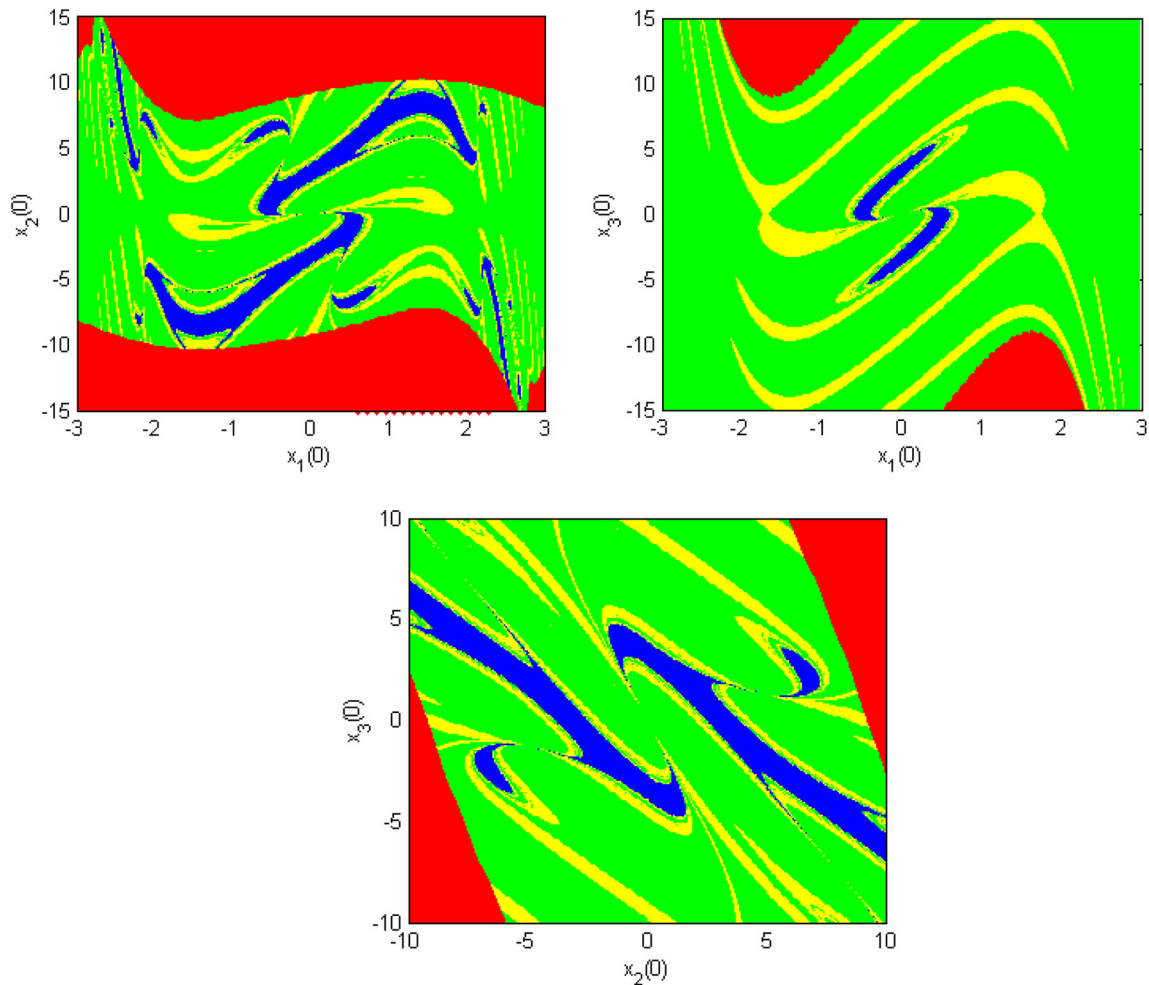
Fig. 15 Cross sections of basins of attraction for $x_3(0) = 0$, $x_2(0) = 0$, and $x_1(0) = 0$ respectively, showing the influence of each attractors of Fig. 14 where the blue basin represents the periodic attractor, those in green and yellow the different chaotic attractors, and the red areas denote the unbounded dynamics obtained for the same set of parameters in Fig. 14

corresponds to a single initial condition given and it is in this sense that we have explored in literature different types of attractors (fixed point, periodic, quasi-periodic, chaotic, and hyperchaotic) that coexist [49]. Considering the bifurcation diagram of Fig. 3, hysteresis windows are observed in the $0.285 \leq \beta \leq 0.208$ and $0.83 \leq \beta \leq 0.86$ ranges. It is obvious that there is a coexistence of two different attractors in the first zone and when the bifurcation diagram of Fig. 3 is widened in the second range as in Fig. 9, a coexistence of several kings of four types of attractors of different natures only by varying only the initial conditions (see Fig. 13). Similarly, when widening the bifurcation diagram and the graph of Lyapunov exponents of Fig. 6 in the range $4.23 \leq \alpha \leq 4.50$, a coexistence of three symmetrical solutions are observed, including the bifurcation like sequence of local maxima of x_1 versus the initial conditions $x_1(0)$ (keeping the other initial variables $x_2(0) = 2$, $x_3(0) = 5$) of Fig. 10(a). We can have a coexistence of two chaotic attractors with a periodic attractor of

period-1 (see Fig. 14) or a coexistence of two periodic attractors with a chaotic attractor ($\alpha = 4.44$ for example).

In the same line, a coexistence of six asymmetric solutions is obtained when widening the bifurcation diagram of Fig. 7 as illustrated in Fig. 11(a) and for a set of initial values of Fig. 11(b), the zoom of the bifurcation diagram of Fig. 11(c) is shown where three branches of different bifurcations can be easily observed in accordance with the initial conditions of Fig. 11(b) a sample of this coexistence of six attractors is presented in Fig. 16.

To illustrate the different coexistence mentioned above, Fig. 12 shows a coexistence of two symmetrical attractors (chaotic in (a) with a limit cycle of period-1 in (b)) for $\beta = 0.3$. The coexistence of four asymmetric attractors are illustrated in Fig. 13 where we respectively have four chaotic attractors of Fig. 13(a_1) and (b_1) for $\beta = 0.8425$, two chaotic attractors (a_2) with two periodic attractors of period-3 (b_2), and finally a coexistence of four periodic attractors (of period-4 (a_3) and period-3 (b_3)). Other works
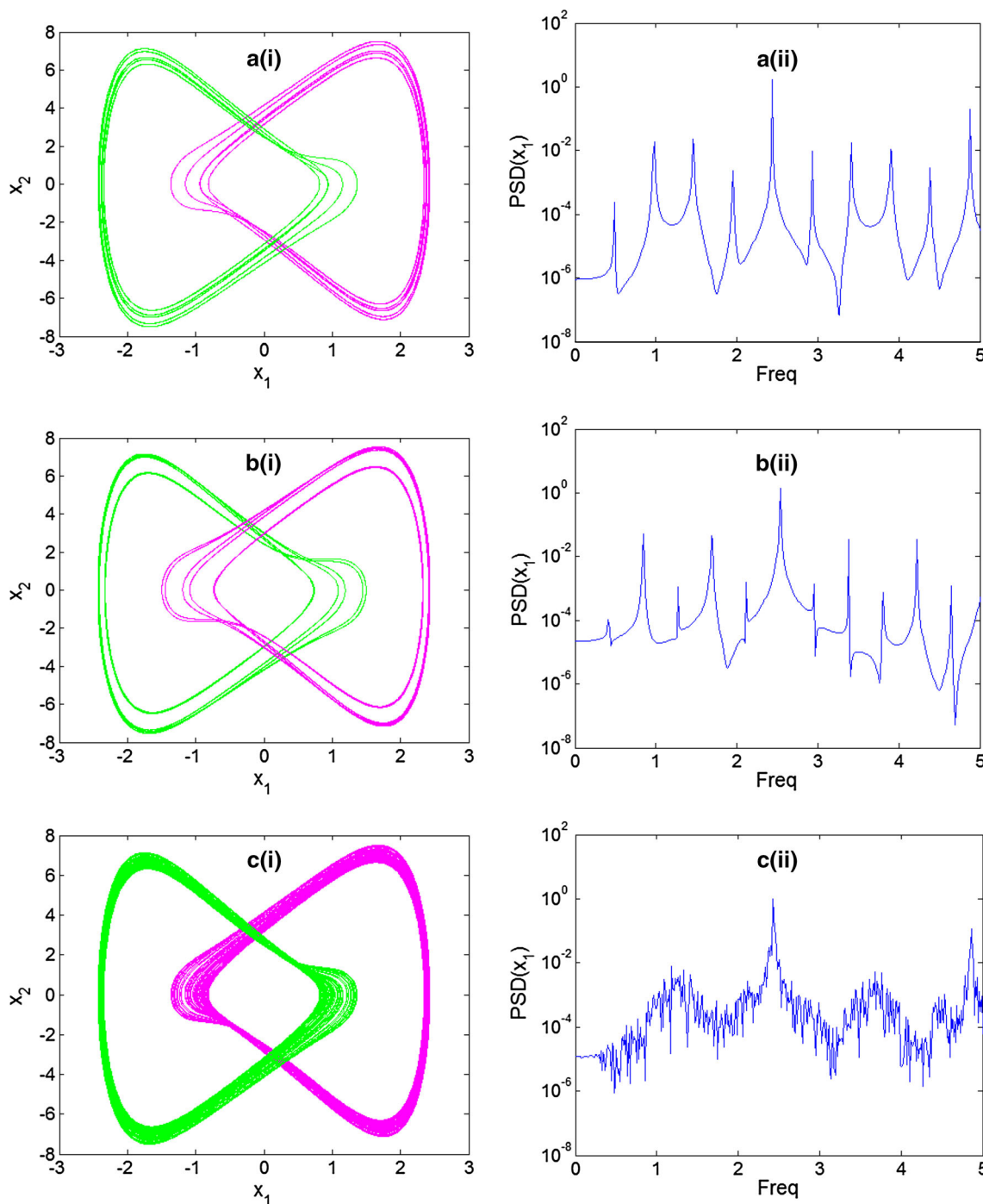
Fig. 16 Phase portraits in the (x_1, x_2) plan and their corresponding spectral power density obtained for the parameters of the system $\beta = 0.7$, $\alpha = 1$, $\gamma = 0.5$, $\rho = 1$, and $a = 7.42$ illustrating the coexistence of six asymmetrical solutions: **a** two limits cycle of period-5, **b** two limits cycle of period-6, with two chaotic attractors **c**. Initial conditions are $(0, 0.375, 0)$,$(0, 0.15, 0)$, and $(0, 0.8, 0)$ respectively

whose authors also show the coexistence of four different attractors are investigated in [50, 51].

More interestingly, a coexistence of three symmetrical attractors and their correspondence densities spectral of frequency is presented in Fig. 14 where in (a) a limit cycle

of period-1 coexists with two chaotic attractors (b) and (c) (for more detail see caption of the figure). Each attractor of Fig. 14 corresponds to a space that it magnetizes in the phase space of the initial conditions. Thus, cross-section of a basin of attraction (all of the initial conditions that give
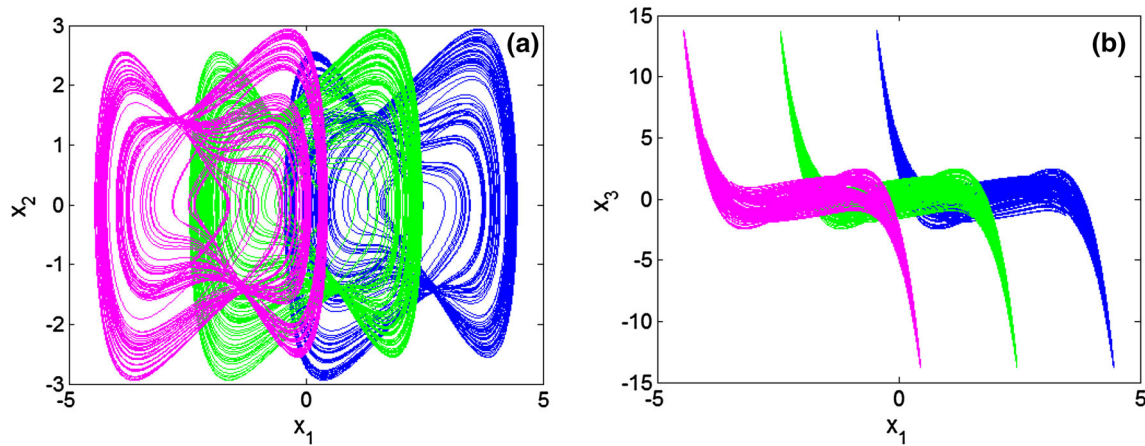
Fig. 17 Offset boosting of the chaotic attractor for varying the control parameter k: in (x_1, x_2) and (x_1, x_3) planes for $k = -2$ (blue), $k = 0$ (green), and $k = 2$ (magenta). Others parameters are $\alpha = 1$, $\beta = 0.8$, $\gamma = 0.5$, and $\rho = 1$

rise to one or another attractor) is presented in Fig. 15 in the $(x_1(0), x_2(0))$, $(x_1(0), x_3(0))$, and $(x_2(0), x_3(0))$ planes of the initial conditions where each color corresponds to a coexisting attractor of Fig. 14 (see caption of Fig. 15).

Figure 16 shows the coexistence of the six attractors and their corresponding frequency diagrams where we can easily distinguish the periodicity of each attractor. This figure presents four periodic attractors (a) and (b) that coexist with the other two chaotic (c) for a set of system parameters $\alpha = 1$, $\beta = 0.7$ $\gamma = 0.5$, $\rho = 1$, and $a = 7.42$ but by varying only the initial condition $x_2(0)$. Several works also explores the coexistence of six solutions in the literature [52, 53].

Another form of coexistence of the attractors is offset boosting [54, 55] which is obtained by varying a single parameter k added to the state variable x_1 ($x_1 + k$). Note that this parameter is not added to hazard and the only condition of its existence is that when a state variable of the system appears on a single line as in [56], it is possible that this system develops the phenomenon of offset boosting. Only the variable x_1 can be booster and thus, for discrete values of k, we have attractors of the same nature that appear in a staggered way. An example of this phenomenon is presented in Fig. 17 where the chaotic attractor has seen booster on several positions (see caption of the figure for the details).
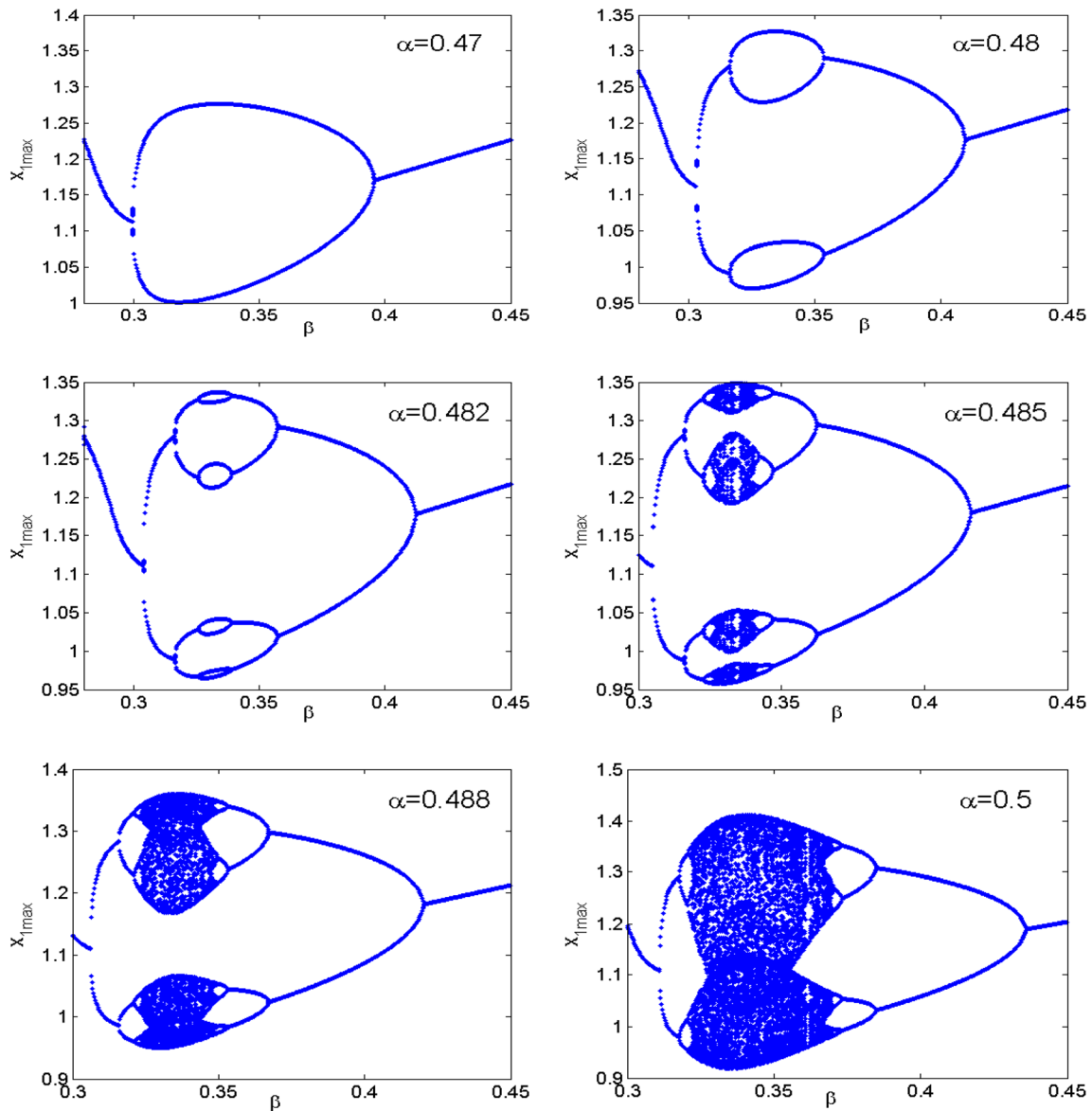
4.4 Antimonotonicity

Next to the multistability which is a strange and unpredictable phenomenon, it exists to the other which is obtained by appearance followed by the spontaneous disappearance of the periodic bubbles of bifurcations. This birth followed by the disappearance of the bifurcation bubbles is called antimonotonicity and is explored in several works namely in [57]. This new phenomenon is

observed in our system (5) and illustrated in Fig. 18 for different discrete values of the parameter α considering β as the bifurcation control parameter (see caption of Fig. 18). To justify the existence of the phenomenon of antimonotonicity observed in our system, we explore the discrete first return map dynamics. From the positions of two critical return points C_1 and C_2 consecutive to $t = t_n$ and $t = t_{n+1}$, we have drawn the diagram of Fig. 19 $(M_{n+1}(x_2) = f(M_n(x_2)))$. Note that the points C_1 and C_2 respectively justify the apparition and destruction of periodic bubble bifurcations [58, 59].

5 Circuit diagram and PSpice results

The purpose of this section is to propose a simple electronics circuit in order to validate the correctness of the proposed model [60]. Since there is no standard memcapacitor circuit in the literature, building an equivalent memcapacitor circuit is a big challenge. In Fig. 20, the memcapacitor-based circuit simulation model is designed, where the proposed charge-controlled memcapacitor is presented by the dotted block. The circuit components of Fig. 20 are in others the operational amplifiers U_1A to U_1D and U_2A of the integrated circuits $TL084$, capacitors C_1 and C_2, the real inductance L with its internal resistance r, the resistors R and R_i for $i = \{1 \ to \ 3\}$, and the multipliers defined by M_1, M_2, and M_3. A symmetric voltage of $\pm 15 \ V$ serves to supply the circuit components. By exploiting the Kirchhoff laws, the differential system describing the dynamics of the circuit of Fig. 20 is obtained as follows:

Fig. 18 Bifurcation diagrams (showing the phenomenon of anti-monotonicity) obtained by plotting the local maxima of the state variable x_1 as a function of the control parameter β: period-2 bubble for $\alpha = 0.47$; period-4 bubble for $\alpha = 0.48$; period-8 bubble for $\alpha = 0.482$; four chaotic bubbles for $\alpha = 0.485$; two chaotic bubbles for $\alpha = 0.488$; Full Feigenbaum remerging tree at $\alpha = 0.5$. The rest of fixed parameters are $\gamma = 0.5$ and $\rho = 1$

$$
\begin{cases}
\dfrac{dv_{C_1}}{dt} = \dfrac{1}{RC} v_{C_2}, \\[2mm]
\dfrac{dv_{C_2}}{dt} = \dfrac{1}{RC} R_0 i_L, \\[2mm]
\dfrac{di_L}{dt} = -\dfrac{r}{L} i_L - \dfrac{1}{L} v_m,
\end{cases}
\tag{11}
$$

where $v_m = -R\left(-\frac{1}{R_2} v_{C_1} + \frac{1}{R_3} v_{C_2} - \frac{1}{R_1} v_{C_1}^4 v_{C_2}\right)$.

To implement the proposed oscillator conveniently, we introduce the scaling factor RC. Thus, by carrying out the variable change $t = \tau RC$, system (11) becomes:

$$
\begin{cases}
\dfrac{dv_{C_1}}{d\tau} = v_{C_2} \\[2mm]
\dfrac{dv_{C_2}}{d\tau} = R_0 i_L \\[2mm]
\dfrac{di_L}{d\tau} = -\dfrac{rRC}{L} i_L - \dfrac{R^2 C}{LR_2} v_{C_1} + \dfrac{R^2 C}{LR_3} v_{C_2} - \dfrac{R^2 C}{LR_1} v_{C_1}^4 v_{C_2}
\end{cases}
\tag{12}
$$

where v_{C_1} and v_{C_2} are the voltages across the capacitors C_1 and C_2; i_L the current of the inductor L. With the following variable change $C_1 = C_2 = C$, $X_1 = v_{C_1}$, $X_2 = v_{C_2}$,
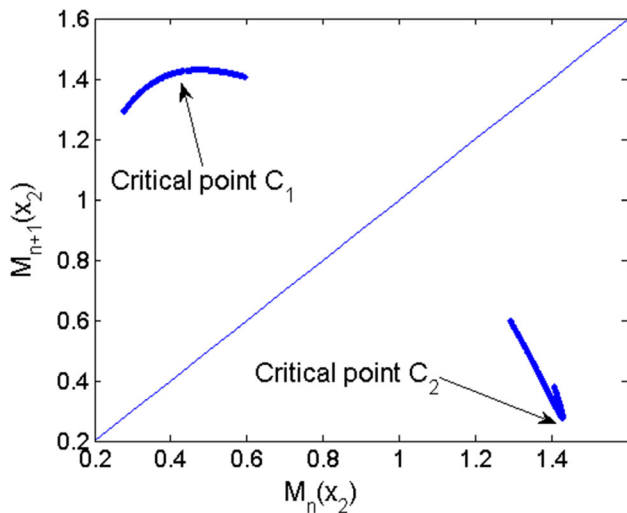
Fig. 19 First-return map of the maxima of the coordinate x_2. This map is indicative of one-dimensional maps with two critical points confirming the occurrence of antimonotonicity in the proposed memcapacitor oscillator. The parameters are: $\alpha = 0.5$, $\beta = 0.34$, $\gamma = 0.5$, and $\rho = 1$

$X_3 = i_L$, $\alpha = \frac{R^2 C}{LR_3}$, $\gamma = \frac{rRC}{L}$, $\beta = \frac{R^2 C}{LR_2}$, $\rho = \frac{R^2 C}{LR_1}$, and $a = R_0$(the added parameter of Sect. 4) the dynamics of the electronic circuit of Fig. 20 and the one of Fig. 2 are equivalents.

The circuit diagram of Fig. 20 is simulated by PSpice software and the complex behaviors are carried out through the phase portraits. For the choice of the resistors $R_1 = 25\Omega$ and $R_2 = 13K\Omega$, we obtain the asymmetric chaotic attractors of Fig. 21. For the resistors $R_1 = 50\Omega$ and $R_2 = 11K\Omega$, we obtain the symmetric chaotic attractors of Fig. 22 on different planes of the system's coordinate. In light of Figs. 21 and 22, a good agreement is observed between the behaviors obtained by PSpice simulations of the left column and those obtained by the numerical resolution of the right column. Obtaining these chaotic behaviors confirms the feasibility of the proposed model, which is justified by the concordance between the results obtained.

6 Conclusion

A novel mathematical model of charge-controlled memcapacitor and its corresponding circuit emulator is introduced in this paper. Based on this model, a simple chaotic oscillator is proposed and studied in detail. The simplicity of the circuit and the complexity of the dynamic behavior are the particular characteristics of the proposed model. The entire dynamics of the system has been explored giving rise to a plethora of phenomena including multistability (through the coexistence of several types of dynamic behavior), antimonotonicity, and offset boosting. For the validation and the feasibility of the model, a circuit realization has been carried out via PSpice simulations whose results are in good agreement. This discovery enriches for this purpose the literature on dynamic systems in general and the family of oscillators based on the charge-controlled memcapacitor, in particular by rich, varied and complex results.
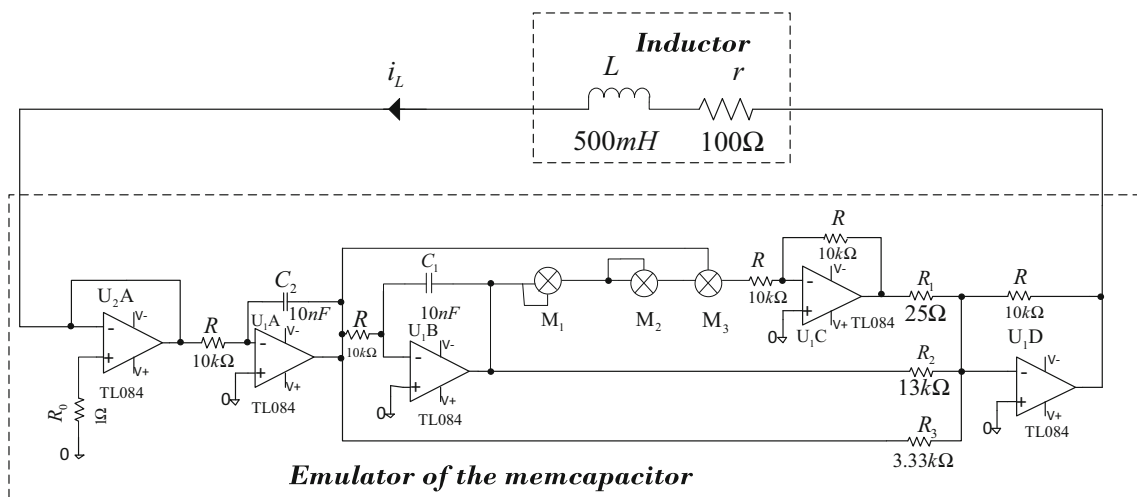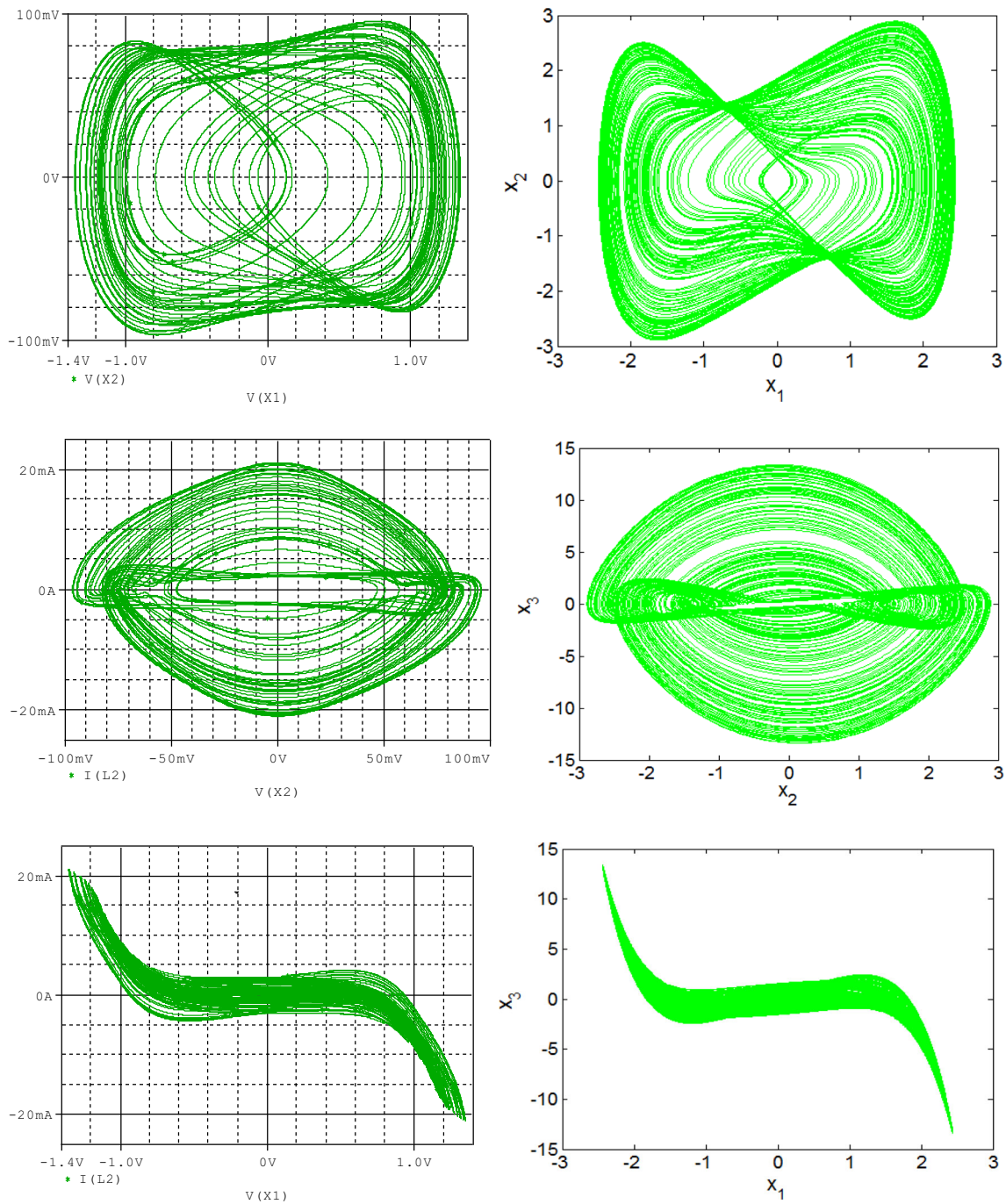

Fig. 20 Circuit realization of the memcapacitor-based chaotic oscillator
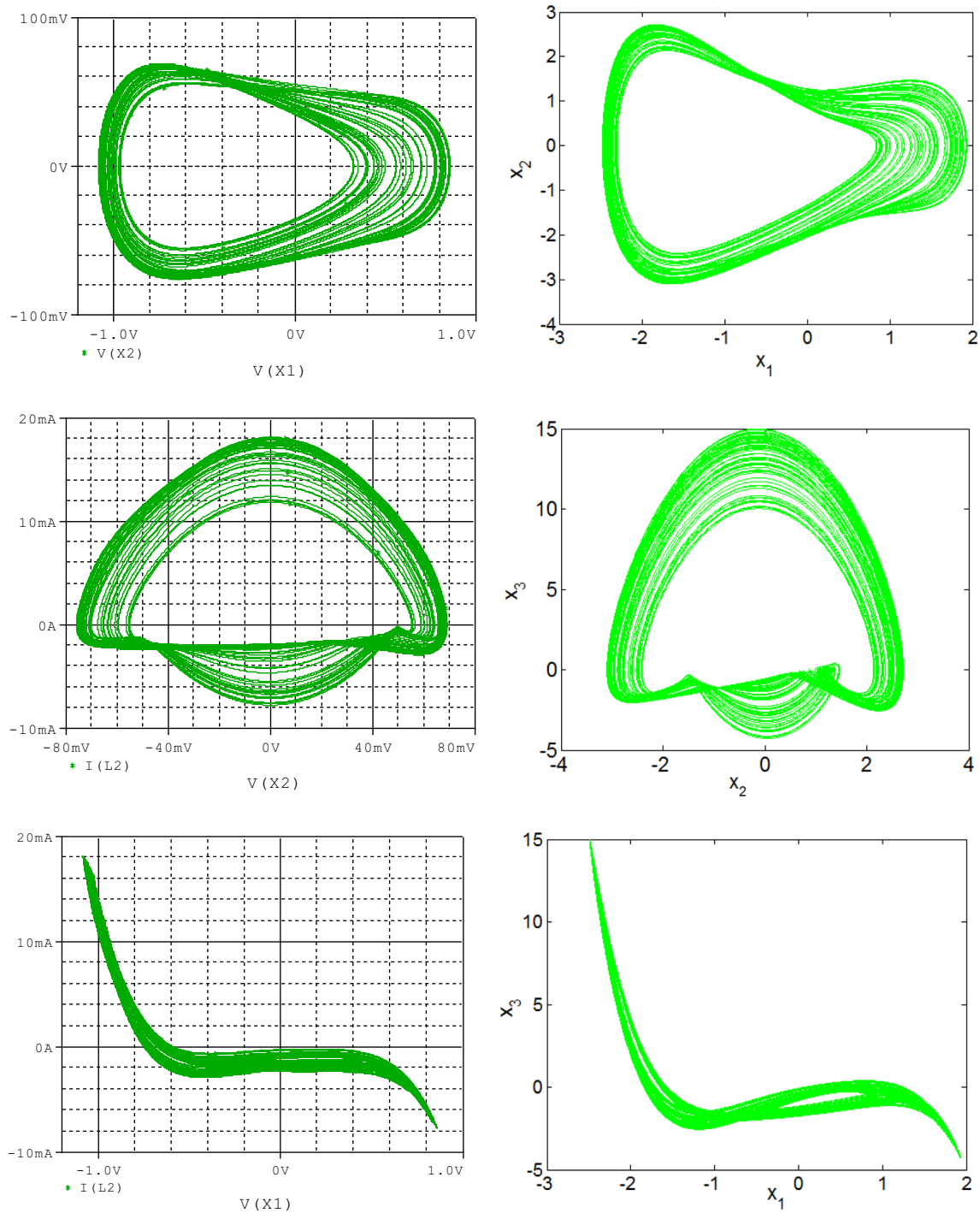
Fig. 21 Asymmetric chaotic attractor in the different planes obtained by PSpice simulations for $R_1 = 25\Omega$ and $R_2 = 13\text{k}\Omega$. The initial conditions $(v_{C_1}(0),\ v_{C_2}(0),\ i_L(0))$ are (0.1, 0, 0)

Fig. 22 Symmetric chaotic attractor in the different planes obtained by PSpice simulations for $R_1 = 50\Omega$ and $R_2 = 11k\Omega$. The initial conditions $(v_{C_1}(0),\ v_{C_2}(0),\ i_L(0)\,)$ are (0.1, 0, 0)

References

1. Chua, L. (1971). Memristor-the missing circuit element. *IEEE Transactions on Circuit Theory, 18*(5), 507–519.
2. Wen, S., Zeng, Z., Huang, T., & Zhang, Y. (2013). Exponential adaptive lag synchronization of memristive neural networks via fuzzy method and applications in pseudorandom number generators. *IEEE Transactions on Fuzzy Systems, 22*(6), 1704–1713.
3. Fouda, M. E., & Radwan, A. G. (2015). Resistive-less memcapacitor-based relaxation oscillator. *International Journal of Circuit Theory and Applications, 43*(7), 959–965.
4. Fouda, M., & Radwan, A. (2012). Charge controlled memristorless memcapacitor emulator. *Electronics Letters, 48*(23), 1454–1455.
5. Sah, M., Yang, C., Budhathoki, R., Kim, H., & Yoo, H. (2013). Implementation of a memcapacitor emulator with off-the-shelf devices. *Elektronika ir elektrotechnika, 19*(8), 54–58.

6. Fouda, M., Khatib, M., & Radwan, A. On the mathematical modeling of series and parallel memcapacitors. In *2013 25th international conference on microelectronics (ICM), 2013* (pp. 1–4). IEEE

7. Di Ventra, M., Pershin, Y. V., & Chua, L. O. (2009). Circuit elements with memory: Memristors, memcapacitors, and meminductors. *Proceedings of the IEEE, 97*(10), 1717–1724.

8. Itoh, M., & Chua, L. O. (2008). Memristor oscillators. *International Journal of Bifurcation and Chaos, 18*(11), 3183–3206.

9. Muthuswamy, B., & Chua, L. O. (2010). Simplest chaotic circuit. *International Journal of Bifurcation and Chaos, 20*(05), 1567–1580.

10. Zhong, G.-Q. (1994). Implementation of Chua's circuit with a cubic nonlinearity. *IEEE Transactions on Circuits and Systems I: Fundamental Theory and Applications, 41*(12), 934–941.

11. Wang, G., Zang, S., Wang, X., Yuan, F., & Iu, H. H.-C. (2017). Memcapacitor model and its application in chaotic oscillator with memristor. *Chaos: An Interdisciplinary Journal of Nonlinear Science, 27*(1), 013110.

12. Buscarino, A., Fortuna, L., Frasca, M., & ValentinaGambuzza, L. (2012). A chaotic circuit based on Hewlett-Packard memristor. *Chaos An Interdisciplinary Journal of Nonlinear Science, 22*(2), 023136.

13. Corinto, F., Krulikovskyi, V., & Haliuk, S. D. Memristor-based chaotic circuit for pseudo-random sequence generators. In *2016 18th Mediterranean electrotechnical conference (MELECON), 2016* (pp. 1–3). IEEE

14. Kountchou, M., Louodop, P., Bowong, S., & Fotsin, H. (2016). Analog circuit design and optimal synchronization of a modified Rayleigh system. *Nonlinear Dynamics, 85*(1), 399–414.

15. Fitch, A. L., Iu, H. H., & Yu, D. Chaos in a memcapacitor based circuit. In *2014 IEEE international symposium on circuits and systems (ISCAS), 2014* (pp. 482–485). IEEE.

16. Hu, Z., Li, Y., Jia, L., & Yu, J. Chaos in a charge-controlled memcapacitor circuit. In *2010 international conference on communications, circuits and systems (ICCCAS), 2010* (pp. 828–831). IEEE

17. Wang, G.-Y., Jin, P.-P., Wang, X.-W., Shen, Y.-R., Yuan, F., & Wang, X.-Y. (2016). A flux-controlled model of meminductor and its application in chaotic oscillator. *Chinese Physics B, 25*(9), 090502.

18. Zhu, H., Duan, S., Wang, L., Yang, T., & Tan, J. The nonlinear meminductor models with its study on the device parameters variation. In *2017 seventh international conference on information science and technology (ICIST), 2017* (pp. 497–503). IEEE.

19. Yu, D., Liang, Y., Chen, H., & Iu, H. H. (2013). Design of a practical memcapacitor emulator without grounded restriction. *IEEE Transactions on Circuits and Systems II: Express Briefs, 60*(4), 207–211.

20. Wang, X., Fitch, A., Iu, H., & Qi, W. (2012). Design of a memcapacitor emulator based on a memristor. *Physics Letters A, 376*(4), 394–399.

21. Liang, Y., Yu, D.-S., & Chen, H. (2013). A novel meminductor emulator based on analog circuits. *Acta Physica Sinica, 62*(15), 158501.

22. Vista, J., & Ranjan, A. (2020). Simple charge controlled floating memcapacitor emulator using DXCCDITA. *Analog Integrated Circuits and Signal Processing, 104*(1), 37–46.

23. Vista, J., & Ranjan, A. design of memcapacitor emulator using DVCCTA. In *Journal of Physics: Conference Series, 2019* (Vol. 1172, pp. 012104). IOP Publishing.

24. Yu, D., Liang, Y., Iu, H. H., & Chua, L. O. (2014). A universal mutator for transformations among memristor, memcapacitor, and meminductor. *IEEE Transactions on Circuits and Systems II: Express Briefs, 61*(10), 758–762.

25. Pershin, Y. V., & Di Ventra, M. (2011). Emulation of floating memcapacitors and meminductors using current conveyors. *Electronics Letters, 47*(4), 243–244.

26. Yuan, F., Wang, G., & Wang, X. (2017). Chaotic oscillator containing memcapacitor and meminductor and its dimensionality reduction analysis. *Chaos An Interdisciplinary Journal of Nonlinear Science, 27*(3), 033103.

27. Wang, X., Yu, J., Jin, C., Iu, H. H. C., & Yu, S. (2019). Chaotic oscillator based on memcapacitor and meminductor. *Nonlinear Dynamics, 96*(1), 161–173.

28. Yuan, F., Li, Y., Wang, G., Dou, G., & Chen, G. (2019). Complex dynamics in a memcapacitor-based circuit. *Entropy, 21*(2), 188.

29. Xu, B., Wang, G., & Shen, Y. (2017). A simple meminductor-based chaotic system with complicated dynamics. *Nonlinear Dynamics, 88*(3), 2071–2089.

30. Negou, A. N., & Kengne, J. (2019). A minimal three-term chaotic flow with coexisting routes to chaos, multiple solutions, and its analog circuit realization. *Analog Integrated Circuits and Signal Processing, 101*(3), 415–429.

31. Tchitnga, R., Fotsin, H. B., Nana, B., Fotso, P. H. L., & Woafo, P. (2012). Hartley's oscillator: The simplest chaotic two-component circuit. *Chaos, Solitons & Fractals, 45*(3), 306–313.

32. Tchitnga, R., Nguazon, T., Fotso, P. H. L., & Gallas, J. A. (2015). Chaos in a single op-amp–based jerk circuit: Experiments and simulations. *IEEE Transactions on Circuits and Systems II: Express Briefs, 63*(3), 239–243.

33. Joshi, M., & Ranjan, A. (2019). New simple chaotic and hyper-chaotic system with an unstable node. *AEU-International Journal of Electronics and Communications, 108*, 1–9.

34. Joshi, M., & Ranjan, A. (2020). An autonomous simple chaotic jerk system with stable and unstable equilibria using reverse sine hyperbolic functions. *International Journal of Bifurcation and Chaos, 30*(05), 2050070.

35. Joshi, M., & Ranjan, A. (2020). Investigation of dynamical properties in hysteresis-based a simple chaotic waveform generator with two stable equilibrium. *Chaos, Solitons & Fractals, 134*, 109693.

36. Sprott, J. C. (2011). A proposed standard for the publication of new chaotic systems. *International Journal of Bifurcation and Chaos, 21*(09), 2391–2394.

37. Ma, X., Mou, J., Liu, J., Ma, C., Yang, F., & Zhao, X. (2020). A novel simple chaotic circuit based on memristor–memcapacitor. *Nonlinear Dynamics, 100*, 2859–2876.

38. Chua, L. O. (2005). Local activity is the origin of complexity. *International Journal of Bifurcation and Chaos, 15*(11), 3435–3456.

39. Signing, V. F., & Kengne, J. (2018). Coexistence of hidden attractors, 2-torus and 3-torus in a new simple 4-D chaotic system with hyperbolic cosine nonlinearity. *International Journal of Dynamics and Control, 6*(4), 1421–1428.

40. Signing, V. F., Kengne, J., & Kana, L. (2018). Dynamic analysis and multistability of a novel four-wing chaotic system with smooth piecewise quadratic nonlinearity. *Chaos, Solitons & Fractals, 113*, 263–274.

41. Signing, V. F., & Kengne, J. (2019). Reversal of period-doubling and extreme multistability in a novel 4D chaotic system with hyperbolic cosine nonlinearity. *International Journal of Dynamics and Control, 7*(2), 439–451.

42. Kengne, J., Njikam, S., & Signing, V. F. (2018). A plethora of coexisting strange attractors in a simple jerk system with hyperbolic tangent nonlinearity. *Chaos, Solitons & Fractals, 106*, 201–213.

43. Yadav, V. K., Das, S., Bhadauria, B. S., Singh, A. K., & Srivastava, M. (2017). Stability analysis, chaos control of a fractional order chaotic chemical reactor system and its function

projective synchronization with parametric uncertainties. *Chinese Journal of Physics, 55*(3), 594–605.

44. Noube, M. K., Louodop, P., Bowong, S., & Fotsin, H. (2014). Optimization of the synchronization of the modified Duffing system. *Journal of Advanced Research, 6*(2), 25–48.

45. Pone, J. R. M., Tamba, V. K., Kom, G. H., & Tiedeu, A. B. (2019). Period-doubling route to chaos, bistability and anti-mononicity in a jerk circuit with quintic nonlinearity. *International Journal of Dynamics and Control, 7*(1), 1–22.

46. Wolf, A., Swift, J. B., Swinney, H. L., & Vastano, J. A. (1985). Determining Lyapunov exponents from a time series. *Physica D: Nonlinear Phenomena, 16*(3), 285–317.

47. Argyris, J. H., Faust, G., Haase, M., & Friedrich, R. (2015). *An exploration of dynamical systems and chaos: Completely revised and enlarged* (2nd ed.). Berlin: Springer.

48. Alombah, N. H., Fotsin, H., & Romanic, K. (2017). Coexistence of multiple attractors, metastable chaos and bursting oscillations in a multiscroll memristive chaotic circuit. *International Journal of Bifurcation and Chaos, 27*(05), 1750067.

49. Lai, Q., Akgul, A., Varan, M., Kengne, J., & Erguzel, A. T. (2018). Dynamic analysis and synchronization control of an unusual chaotic system with exponential term and coexisting attractors. *Chinese Journal of Physics, 56*(6), 2837–2851.

50. Kengne, J., Tsafack, N., & Kengne, L. K. (2018). Dynamical analysis of a novel single Opamp-based autonomous LC oscillator: Antimonotonicity, chaos, and multiple attractors. *International Journal of Dynamics and Control, 6*(4), 1543–1557.

51. Negou, A. N., & Kengne, J. (2018). Dynamic analysis of a unique jerk system with a smoothly adjustable symmetry and nonlinearity: Reversals of period doubling, offset boosting and coexisting bifurcations. *AEU-International Journal of Electronics and Communications, 90*, 1–19.

52. Tsafack, N., & Kengne, J. (2018). A novel autonomous 5-d hyperjerk RC circuit with hyperbolic sine function. *The Scientific World Journal, 2018*.

53. Lai, Q., Nestor, T., Kengne, J., & Zhao, X.-W. (2018). Coexisting attractors and circuit implementation of a new 4D chaotic system with two equilibria. *Chaos, Solitons & Fractals, 107*, 92–102.

54. Tagne, R. M., Kengne, J., & Negou, A. N. (2019). Multistability and chaotic dynamics of a simple Jerk system with a smoothly tuneable symmetry and nonlinearity. *International Journal of Dynamics and Control, 7*(2), 476–495.

55. Kengne, J., & Kengne, L. K. (2019). Scenario to chaos and multistability in a modified Coullet system: Effects of broken symmetry. *International Journal of Dynamics and Control, 7*(4), 1225–1241.

56. Pham, V.-T., Volos, C., Jafari, S., & Kapitaniak, T. (2017). Coexistence of hidden chaotic attractors in a novel no-equilibrium system. *Nonlinear Dynamics, 87*(3), 2001–2010.

57. Dawson, S. P., Grebogi, C., Yorke, J. A., Kan, I., & Koçak, H. (1992). Antimonotonicity: Inevitable reversals of period-doubling cascades. *Physics Letters A, 162*(3), 249–254.

58. Leutcho, G. D., & Kengne, J. (2018). A unique chaotic snap system with a smoothly adjustable symmetry and nonlinearity: Chaos, offset-boosting, antimonotonicity, and coexisting multiple attractors. *Chaos, Solitons & Fractals, 113*, 275–293.

59. Signing, V. F., Kengne, J., & Pone, J. M. (2019). Antimonotonicity, chaos, quasi-periodicity and coexistence of hidden attractors in a new simple 4-D chaotic system with hyperbolic cosine nonlinearity. *Chaos, Solitons & Fractals, 118*, 187–198.

60. Zhang, S., Zeng, Y., & Li, Z. (2018). One to four-wing chaotic attractors coined from a novel 3D fractional-order chaotic system with complex dynamics. *Chinese Journal of Physics, 56*(3), 793–806.

Michaux Kountchou was born in Bertoua, Cameroon, in 1981. He received his M.Sc. and Ph.D. degrees in Electronics from the Faculty of Sciences, University of Dschang, Cameroun. He worked as a researcher at the Nuclear Technology Section, Institute of Geological and Mining Research, Yaounde, Cameroun. Dr. Michaux Kountchou has authored or co-authored several journal papers. He also serves as reviewer for renowned international journals including AEÜ - International Journal of Electronics and Communications, Chinese Journal of Physics, Nonlinear Dynamics. His current research interests include, nonlinear systems and circuits, chaos, multistability, optimal control and synchronisation with applications. He also conducts research in the field of nuclear instrumentation with a view to developing new methods, tools, efficient hardware and software necessary for the maintenance, repair and calibration of radiation detection equipment.

Vitrice Ruben Folifack Signing was born in Kribi, Cameroun, in 1989. He is a researcher at the Nuclear Technology Section, Institute of Geological and Mining Research, Yaounde, Cameroon. He received his M.Sc. in Physics/Electronics from the University of Dschang, Cameroon, under the advisory of Prof. Jacques Kengne in 2016. He is a PhD Student at University of Dschang, under the advisory of Prof. Jacques Kengne. His research interest includes nonlinear systems and circuits, chaos, multistability, chaos-based applications. Also develops new and effective methods, tools, hardware and software necessary for the maintenance, repair, and calibration of radiation detection equipment. Their current projects are 'Hidden oscillations' and 'self-excited oscillations'.
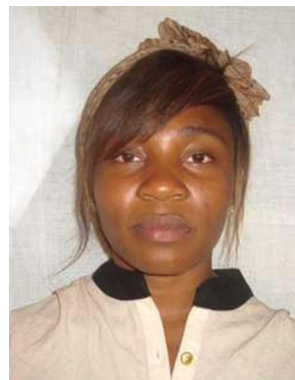
Ruth Line Tagne Mogue was born in Bafoussam, Cameroun, in 1995. She is a researcher at the Nuclear Technology Section, Institute of Geological and Mining Research, Yaounde, Cameroon. She received his M.Sc. in Physics/Electronics from the University of Dschang, Cameroon, under the advisory of Prof. Hilaire Fotsin in 2017. She is a PhD Student at University of Dschang, under the advisory of Prof. Jacques Kengne. Her research interest includes nonlinear systems and circuits, chaos, multistability, chaos-based applications. Also develops new and effective methods, tools,

hardware and software necessary for the maintenance, repair, and calibration of radiation detection equipment.

Jacques Kengne was born in Bamougoum, Cameroon, in 1971. He received his M.Sc., and Ph. D. degrees in Electronics in 2007 and 2011 respectively from the Faculty of Sciences/University of Dschang. From 2010 to 2012, he worked as a lecturer at the Department of Electrical Engineering, IUT-FV/University of Dschang. From 2012 to 2016 he served as senior Lecturer. In 2016, he was appointed Associated-Professor in the same University. Prof. Kengne Jacques has authored or co-authored more than 60 journal papers. He also serves as reviewer for renowned international journals including IJBC, Nonlinear Dynamics, Chaos solitons and fractals, and IEEE Trans Circuits Systems. His research interest includes nonlinear systems and circuits, chaos, multistability, chaos synchronization with applications.

Saïdou is Associate Professor of Nuclear Physics, Dosimetry and Radiation Protection at the Physics Department, Faculty of Science, University of Yaounde I. He is the Section Head of the Nuclear Technology Section, Institute of Geological and Mining Research since 2008. He carried out his PhD work at the Institute of Radiation Physics, University of Lausanne from October 2004 to October 2007. He got his PhD degree on November 2007 at the Centre for Atomic Molecular Physics and Quantum Optics, University of Douala, Cameroon. He is currently leading some Technical Cooperation Projects funded by the International Atomic Energy Agency. He is the Founder and President of the Cameroon Radiation Protection Society, affiliated to the International Radiological Protection Association (IRPA) since 2013, as 49th IRPA Associate Society.